

Observation of Negative Absolute Resistance in a Josephson Junction

J. Nagel,¹ D. Speer,² T. Gaber,¹ A. Sterck,¹ R. Eichhorn,² P. Reimann,² K. Ilin,³ M. Siegel,³ D. Koelle,¹ and R. Kleiner^{1,*}

¹*Physikalisches Institut – Experimentalphysik II and Center for Collective Quantum Phenomena and their Applications, Universität Tübingen, Auf der Morgenstelle 14, D-72076 Tübingen, Germany*

²*Fakultät für Physik, Universität Bielefeld, 33615 Bielefeld, Germany*

³*Institut für Mikro- und Nanoelektronische Systeme, Universität Karlsruhe (TH), Hertzstraße 16, D-76187 Karlsruhe, Germany*

(Received 24 January 2008; published 29 May 2008)

We experimentally demonstrate the occurrence of negative absolute resistance (NAR) up to about -1Ω in response to an externally applied dc current for a shunted Nb-Al/ AlO_x -Nb Josephson junction, exposed to a microwave current at frequencies in the GHz range. The realization (or not) of NAR depends crucially on the amplitude of the applied microwave current. Theoretically, the system is described by means of the resistively and capacitively shunted junction model in terms of a moderately damped, classical Brownian particle dynamics in a one-dimensional potential. We find excellent agreement of the experimental results with numerical simulations of the model.

DOI: [10.1103/PhysRevLett.100.217001](https://doi.org/10.1103/PhysRevLett.100.217001)

PACS numbers: 74.50.+r, 05.45.-a, 05.40.-a, 05.60.Cd

When a static force is applied to a system consisting of mobile particles, these particles usually move in the direction of the force, i.e., they show positive mobility, which leads to, e.g., a positive conductance or resistance in electrical systems. Also well known is the fact that such a system can exhibit regions of negative differential mobility or resistance [1–6]. However, the absolute mobility or resistance usually remains positive. The opposite response, i.e., a motion against the static force is termed negative absolute mobility or negative absolute resistance (NAR). This is clearly a quite counter intuitive effect which, at first glance, might seem even to be in conflict with Newton's laws and thermodynamic principles [7]. Yet, nonlinear systems being driven far from equilibrium can indeed exhibit not only a negative differential resistance but also a NAR effect. Unambiguous and convincing experimental observations of NAR are still quite scarce, involving systems consisting of electrons in a sample of bulk GaAs [8], electrons in semiconductor heterostructures [9], electrons in low dimensional conductors [10], and charged Brownian particles in structured microfluidic devices [11]. Apart from the low dimensional conductors, the system was always driven out of equilibrium by means of an ac driving force and then its response to an externally applied static perturbation was studied. On the theoretical side, a considerably larger literature is available, most notably on different types of semiconductors and semiconductor heterostructures [7]. In all those cases (except [11]) NAR is based on purely quantum mechanical effects which cannot be transferred into the realm of classical physics. For classical systems, a first theoretical demonstration of the effect was provided in the context of a spatially periodic and symmetric model system of interacting Brownian particles, subjected to multiplicative white noise [12]. While each of the different ingredients of the model is quite realistic in itself, their combined realization in an experimental system seems difficult. In particular, the main

physical mechanism is based on collective effects of at least three interacting particles [13]. An entirely different mechanism was later on suggested theoretically for a realistic, classical model dynamics of a single Brownian particle in a suitably tailored, two-dimensional potential landscape in Ref. [14] and subsequently realized experimentally in Refs. [11,15]. As a first application of NAR, the separation of different particle species has been realized in Ref. [16]. While the underlying basic physical mechanism still requires at least two spatial dimensions, very recently, NAR has been analyzed and predicted theoretically to occur also in the simplest possible case of a single Brownian particle dynamics in one dimension [17,18]. More precisely, two basically different physical mechanisms capable of generating NAR in such systems have been unraveled, namely, a purely noise induced effect and a transient chaos induced effect [17,18]. In both cases, an experimental realization by means of a Josephson junction subjected to suitable dc and ac currents has been proposed. In this Letter we show that a moderately damped Josephson junction being driven by microwaves indeed shows NAR of the transient chaos induced type. First hints along these lines can be found in Fig. 13 of [19] and in Figs. 12(c) and 14(c) of [20], although without a detailed investigation or discussion of NAR.

To model the Josephson junction we use the resistively and capacitively shunted junction model [21,22]. It describes the equation of motion for the difference δ of the phases of the superconducting order parameter in the two electrodes

$$I = \frac{\Phi_0}{2\pi} C \ddot{\delta} + \frac{\Phi_0}{2\pi R} \dot{\delta} + I_0 \sin \delta + I_N. \quad (1)$$

Here, C , R , and I_0 denote the junction capacitance, resistance and maximum Josephson current, respectively, dots indicate time-derivatives, Φ_0 is the magnetic flux quantum, and $I = I_{\text{dc}} + I_{\text{ac}} \sin(\omega t)$ is the total current applied to the

junction, consisting of a dc and a high frequency ac component. The first term on the right-hand side of Eq. (1) describes the displacement current $C\dot{U}$, where U is the voltage across the junction, and has been rewritten in terms of $\dot{\delta}$ using the Josephson relation $\dot{\delta} = 2\pi U/\Phi_0$. The second term describes the current through the resistor R , the third term the Josephson current, and the last term the noise current arising from Nyquist noise in the resistor. Its spectral power density is assumed to be white with $S_I(f) = 4k_B T/R$, where T is the temperature and k_B Boltzmann's constant. The model (1) implicitly assumes that magnetic fields created by circulating supercurrents can be neglected (short junction limit). This holds when the lateral junction dimensions are below about $4\lambda_J$, where $\lambda_J = (\Phi_0/4\pi\mu_0 j_0 \lambda_L)^{1/2}$ is the Josephson length in terms of the critical current density j_0 , the London penetration depth λ_L , and the magnetic permeability μ_0 .

By integrating Eq. (1) one obtains δ and, by time averaging (we integrate over typically $5 \cdot 10^3$ periods of the ac current), the dc voltage $V = \Phi_0 \langle \dot{\delta} \rangle / 2\pi$ across the junction. This is the main observable of our present work, which is measured when recording $V(I_{dc})$, the current-voltage (I - V) characteristics. For numerical simulations, (1) can be rewritten in dimensionless units by normalizing currents to I_0 , voltages to $I_0 R$, times to $t_c = \Phi_0 / (2\pi I_0 R)$, and hence frequencies to $f_c = I_0 R / \Phi_0$, yielding

$$i = \beta_c \ddot{\delta} + \dot{\delta} + \sin \delta + i_N, \quad (2)$$

where $i = i_{dc} + i_{ac} \sin(\tau f / f_c)$ is the normalized applied current, $\tau = t/t_c$ the normalized time, $\beta_c = (f_c / f_{pl})^2 = 2\pi I_0 R^2 C / \Phi_0$ the Stewart-McCumber parameter, $f_{pl} = [I_0 / (2\pi \Phi_0 C)]^{1/2}$ the Josephson plasma frequency, and i_N the normalized noise current with spectral density $S_i(f/f_c) = 4\Gamma$ and noise parameter $\Gamma = 2\pi k_B T / I_0 \Phi_0$.

For experiments at $T = 4.2$ K, we used circular Nb-Al/AIO_x-Nb Josephson junctions with an area of $200 \mu\text{m}^2$ cf. upper left inset in Fig. 1(a). The junctions were shunted by an AuPd strip with resistance $R = 1.27 \Omega$ and integrated in a coplanar waveguide. We denote the critical current I_c as the maximum dc current for which $V = 0$. In general, I_c is a function of I_{ac} and fluctuations and thus different from I_0 . By measuring $I_c(I_{ac} = 0)$ and matching it with simulations we determined $I_0 = 197 \mu\text{A}$, yielding $I_0 R = 250 \mu\text{V}$, $f_c = 121$ GHz and $\Gamma = 9 \times 10^{-4}$. The Josephson length is about $40 \mu\text{m}$, i.e., well above the $16 \mu\text{m}$ diameter of our junctions assuring the short junction limit. The design value of the capacitance was 8.24 pF, yielding $f_{pl} = 43$ GHz, and $\beta_c = 7.9$. The actual value used in the simulations shown below is somewhat smaller, namely $\beta_c = 7.7$, reproducing particularly well the hysteretic I - V characteristics in the absence of microwaves. The transport measurements have been performed with a standard four terminal method, using filtered leads. Microwaves between 8 and 35 GHz, with variable output power P_m , were applied through a semi-rigid cable that was capacitively coupled to the 50Ω

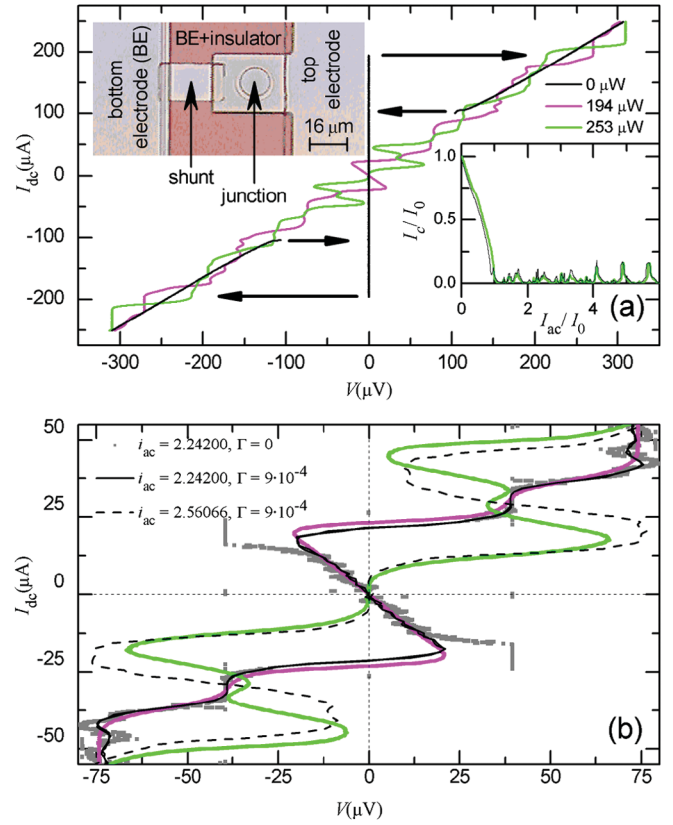


FIG. 1 (color). Current-voltage (I - V) characteristics of the Josephson junction at 4.2 K in a 19 GHz microwave field. (a) I - V characteristics at 3 levels of applied microwave power (0, 194, and 253 μW) showing the effect of negative absolute resistance at 194 μW ($I_{ac} = 435 \mu\text{A}$) and of negative differential resistance at 253 μW ($I_{ac} = 497 \mu\text{A}$). Left inset: optical microscope image of the Josephson junction. Right inset: measured (thick green) and calculated (thin black) dependence of the critical current I_c on the microwave current amplitude I_{ac} . (b) Enlargement of the measured I - V characteristics for 194 μW and 253 μW , together with the simulated I - V characteristics, based on the model dynamics (2) with parameter values as specified in the figure legend and the main text.

coplanar waveguide. The samples were electromagnetically shielded and surrounded by a cryoperm shield, to reduce static magnetic fields.

Given I_0 , R , C , T , and I_{dc} , all relevant model parameters are fixed, with the exception of the (frequency dependent) coupling factor between the microwave amplitude $\sqrt{P_m}$ applied from the source and the amplitude I_{ac} of the ac current induced across the junction. We have fixed this factor by comparing the measured dependence of $I_c(\sqrt{P_m})$ with the calculated curve $I_c(I_{ac})$, as shown in the right inset of Fig. 1, for a microwave frequency of 19 GHz ($f/f_c \approx 0.16$). The experimental and theoretical curves are in good agreement. In particular, the main side maxima can be found, both in experiment and simulation. Adjusting the position of these maxima yields a coupling factor $I_{ac}/\sqrt{P_m}(19 \text{ GHz}) = 1.0 \text{ mA}/\sqrt{\text{mW}}$.

Figure 1(a) shows I - V characteristics under $f = 19$ GHz microwave irradiation at three values of I_{ac} . In the absence of microwaves (black line) the I - V characteristics is hysteretic, with $I_c = 195 \mu\text{A}$ and a return current of $100 \mu\text{A}$ (black arrows). When the microwave field is applied, the hysteresis decreases with increasing I_{ac} , and steplike features appear on the I - V characteristics. At $P_m = 194 \mu\text{W}$ ($I_{ac} = 435 \mu\text{A}$; magenta line), we observe NAR with a resistance of -1.07Ω , occurring in an interval $|I_{dc}| \leq 20 \mu\text{A}$ (i.e., $\approx 10\%$ of I_0). When I_{ac} is increased to $P_m = 253 \mu\text{W}$ ($I_{ac} = 497 \mu\text{A}$; green line) the NAR has disappeared. However, centered on a voltage which corresponds to the first Shapiro step ($V_1 = \Phi_0 f \approx 39 \mu\text{V}$), regions of negative differential resistance appear. In Fig. 1(b) measured and simulated I - V characteristics for the two microwave amplitudes 435 and 497 μA are compared. For the former case, which is recorded at the microwave amplitude where the maximum NAR has been observed, the agreement between the experimental and the theoretical curve is nearly perfect. For the latter case some small differences can be seen, although the agreement is still very good.

An intuitive picture of the observed NAR in Fig. 1 can be obtained by looking upon Eq. (2) as the dynamics of a fictitious particle with coordinate δ in a “tilted washboard potential”, experiencing a constant (in time) tilt via i_{dc} and a periodic driving via i_{ac} . For suitable parameter values of β_c , f , and i_{ac} , the unperturbed deterministic dynamics [Eq. (2) with $i_{dc} = 0$ and $i_N = 0$] exhibits symmetric pairs of long-term solutions, transporting the particle in opposite directions. Such solutions are typically “locked” with the periodic driving in the sense that the particle proceeds by n spatial periods along the washboard potential during m temporal driving periods (Shapiro steps). When an external perturbation in the form of a static dc bias i_{dc} is applied, the naively expected effect would be a boost of the particle motion in the dc bias direction. However, a detailed analysis reveals [18] that for specific parameter values of β_c , f , and i_{ac} , the additional energy fed into the particle motion in the dc bias direction may lead to a destabilization of the long-term solution supporting “downhill” transport (i.e., in the direction of the dc bias), while the “uphill” long-term solution (transport *opposite* to the dc bias) remains stable. Basically, for downhill transport the static dc bias accelerates the particle such that it loses its synchronization with the time-periodic driving. As a consequence, the corresponding “locked downhill” solution ceases to exist and the only remaining long-term solution is the one uphill. The remnant of the destabilized solution exhibits so-called transient chaos, hence the name “transient chaos induced NAR” coined in [18].

The gray curve in Fig. 1(b) shows a simulated I - V characteristics for $i_{ac} = 2.242 \mu\text{A}$ and $\Gamma = 0$, i.e., for the noise-free case $i_N = 0$. Two $n/m = -1$ Shapiro steps with transport (i.e. voltage) opposite to the static dc bias are visible at a voltage of $\pm \Phi_0 f \approx \pm 39 \mu\text{V}$, clearly revealing that the nature of the observed NAR is of the above

explained transient chaos induced type. Below $|I_{dc}| \approx 20 \mu\text{A}$ the Shapiro steps are connected by deterministic chaos.

This NAR effect can be found in a wide range of parameters β_c (roughly between 1 and 100) and f (some 10% of f_{pl} up to f_{pl}) [18], but once these parameters are fixed, the realization of NAR requires a careful choice of i_{ac} . This can also be seen from Fig. 2, which compares in more detail the measured and calculated dependence of V on I_{dc} and on I_{ac} , for two frequencies (8 GHz and 19 GHz). Again, the agreement between theory and experiment is very good. For $f = 8$ GHz, the comparison between measured $I_c(\sqrt{P_m})$ and simulated $I_c(I_{ac})$ curves yields a coupling factor $I_{ac}/\sqrt{P_m}(8 \text{ GHz}) = 0.33 \text{ mA}/\sqrt{\text{mW}}$. In the graphs, V is normalized to $\Phi_0 f$, yielding integer values for integer Shapiro steps. Although being “smoothed out” by thermal noise, the occurrence of such Shapiro steps is clearly visible by the dominance of the colors corresponding to integer $V/\Phi_0 f$ values. For increasing I_{dc} , the normalized voltage covers $V/\Phi_0 f = -1$ to 5 for $f = 8$ GHz and -1 to 4 for $f = 19$ GHz. There are at least five I_{ac} intervals where NAR with $V/\Phi_0 f < 0$ appears at $f = 8$ GHz, and three such intervals at $f = 19$ GHz. Note that those regimes are typically accompanied by an adjacent regime with normal resistance at smaller I_{ac} values, as predicted by the theory of transient chaos induced NAR. Within the NAR regimes, the resistance at $I_{dc} = 0$ reaches values up to about -1Ω . In the case of $f = 8$ GHz, the

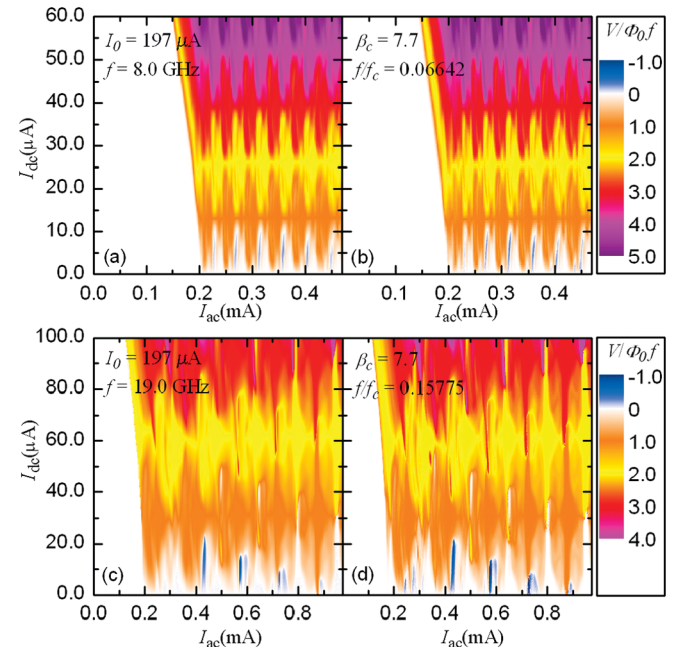


FIG. 2 (color). Contour plot of the normalized dc voltage $V/\Phi_0 f$ across the junction as a function of dc current I_{dc} and microwave current amplitude I_{ac} . (a) $f = 8$ GHz, experiment; (b) $f = 8$ GHz, simulation; (c) $f = 19$ GHz, experiment; (d) $f = 19$ GHz, simulation. For symmetry reasons, $I_{dc} \mapsto -I_{dc}$ implies $V \mapsto -V$, hence negative I_{dc} values are not shown. Blue areas indicate NAR.

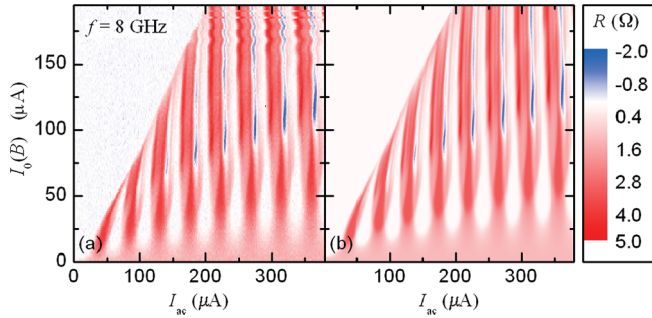


FIG. 3 (color). (a) Contour plot of the experimentally measured resistance $R := V(I = 5 \mu\text{A})/5 \mu\text{A}$ as a function of the Josephson current $I_0(B)$ and of the microwave amplitude I_{ac} . I_0 has been varied by applying a magnetic field to the junction. Graph (b) shows the corresponding simulated plot. For both graphs parameters at $B = 0$ are the same as in Figs. 2(a) and 2(b).

NAR persists up to values of $|I_{dc}| \approx 10 \mu\text{A}$, for all values of I_{ac} for which NAR shows up. In contrast, for $f = 19 \text{ GHz}$, the I_{dc} interval for NAR decreases with increasing I_{ac} . When we increased the frequency further to 35 GHz , hysteretic Shapiro steps appeared on the I - V characteristics, crossing the voltage axis ($I_{dc} = 0$). As a consequence, NAR ceases to exist both in the experiment and the simulations.

In a second series of experiments we applied a magnetic field B parallel to the junction plane in order to tune (decrease) its maximum Josephson current I_0 , making it a B dependent function $I_0(B)$ [23]. Thus all I_0 -dependent parameters in Eq. (2) acquire a B dependence, in particular i , β_c , f/f_c , and Γ . Figure 3 shows a comparison of the measured and calculated dependence of the resistance upon I_{ac} and $I_0(B)$. Again, we find excellent agreement between measurement and theory. Blue regions indicate NAR. Their most remarkable feature is that the values of I_{ac} , for which NAR appears, practically do not depend on I_0 , indicating that the locked solutions on the Shapiro steps within their (parameter) regions of existence are surprisingly insensitive to the height I_0 of the washboard potential barriers [cf. Eq. (1)]. Furthermore, we find that the NAR value can be tuned by I_0 via an applied magnetic field. For our junction parameters we find a maximum NAR for $I_0(B)/I_0(B=0)$ between 0.4 and 0.6; this quantity increases with increasing I_{ac} . At small I_0 values, NAR is not observed in accordance with the fact that for $I_0 \rightarrow 0$ the dynamical Eq. (1) becomes linear such that the total resistance approaches the value of the shunt resistance $R = 1.27 \Omega$.

In conclusion, we have observed negative absolute resistance (NAR) of up to about -1Ω in a shunted Nb-Al/AIO_x-Nb Josephson junction device subjected to microwaves. To clearly see the effect the microwave power needs to be adjusted carefully, but the range of suitable

parameters f and β_c is quite large. In all cases, we obtain very good agreement with theoretical simulations of the resistively and capacitively shunted junction model. The similarity between our Fig. 1 and Fig. 2 in [9] suggests that with respect to NAR, purely quantum mechanical band structure and energy quantization effects may be imitated by inertia effects in a purely classical, one-dimensional noisy dynamics. Moreover, our Fig. 3 exhibits many features which are quite similar to the corresponding plots in [18], while the intuitive explanation of the almost vertical stripe-pattern in Fig. 3 remains as an open problem. As an application, our present work opens the intriguing perspective of a new resistor-type electronic element which is tunable between positive and negative resistance via an easily accessible external control parameter, e.g., the amplitude of an ac driving or an externally applied magnetic field in the mT range.

This work was supported by the Deutsche Forschungsgemeinschaft (KO 1303/7-1, RE 1344/5-1, and SFB 613).

*kleiner@uni-tuebingen.de

- [1] S. R. White and M. Barma, *J. Phys. A* **17**, 2995 (1984).
- [2] G. A. Griess and P. Serwer, *Biopolymers* **29**, 1863 (1990).
- [3] V. Balakrishnan and C. Van den Broeck, *Physica (Amsterdam)* **217A**, 1 (1995).
- [4] G. A. Cecchi and M. O. Magnasco, *Phys. Rev. Lett.* **76**, 1968 (1996).
- [5] G. W. Slater *et al.*, *Phys. Rev. Lett.* **78**, 1170 (1997).
- [6] R. K. P. Zia *et al.*, *Am. J. Phys.* **70**, 384 (2002).
- [7] For a review, see R. Eichhorn *et al.*, *Chaos* **15**, 026113 (2005).
- [8] T. J. Banyas *et al.*, *Sov. Phys. Semicond.* **5**, 1727 (1972).
- [9] B. J. Keay *et al.*, *Phys. Rev. Lett.* **75**, 4102 (1995).
- [10] H. S. J. van der Zant *et al.*, *Phys. Rev. Lett.* **87**, 126401 (2001).
- [11] A. Ros *et al.*, *Nature (London)* **436**, 928 (2005).
- [12] P. Reimann *et al.*, *Europhys. Lett.* **45**, 545 (1999).
- [13] C. Van den Broeck *et al.*, *Int. J. Mod. Phys. C* **13**, 1195 (2002).
- [14] R. Eichhorn *et al.*, *Phys. Rev. Lett.* **88**, 190601 (2002); *Phys. Rev. E* **66**, 066132 (2002); *Physica (Amsterdam)* **325A**, 101, 2003.
- [15] R. Eichhorn *et al.*, *Eur. J. Phys. Special Topics* **143**, 159 (2007); J. Regtmeier *et al.*, *J. Sep. Sci.* **30**, 1461 (2007).
- [16] J. Regtmeier *et al.*, *Eur. Phys. J. E* **22**, 335 (2007).
- [17] L. Machura *et al.*, *Phys. Rev. Lett.* **98**, 040601 (2007); M. Kostur *et al.*, *Phys. Rev. B* **77**, 104509 (2008).
- [18] D. Speer *et al.*, *Europhys. Lett.* **79**, 10005 (2007); *Phys. Rev. E* **76**, 051110 (2007).
- [19] N. F. Pedersen *et al.*, *J. Low Temp. Phys.* **38**, 1 (1980).
- [20] C. Noeldke *et al.*, *J. Low Temp. Phys.* **64**, 235 (1986).
- [21] W. C. Stewart, *Appl. Phys. Lett.* **12**, 277 (1968).
- [22] D. E. McCumber, *J. Appl. Phys.* **39**, 3113 (1968).
- [23] A. Barone and G. Paterno, *Physics and Application of the Josephson Effect* (John Wiley & Sons, New York, 1982).